IEEE Photonics Journal
An IEEE Photonics Society Publication

Open Access

Laser Thermal Tuning by Transient Analytical Analysis of Peltier Device

Volume 9, Number 3, June 2017

Yahya Sheikhnejad
Ricardo Bastos
Zoran Vujicic
Ali Shahpari
Antonio Teixeira

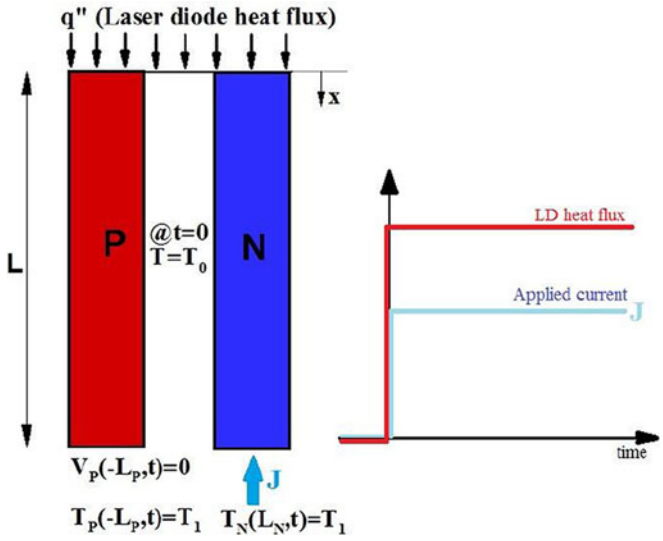

DOI: 10.1109/JPHOT.2017.2695522
1943-0655 © 2017 IEEE

Laser Thermal Tuning by Transient Analytical Analysis of Peltier Device

Yahya Sheikhnejad, Ricardo Bastos, Zoran Vujicic, Ali Shahpari, and Antonio Teixeira

Departamento de Eletrónica, Telecomunicações e Informática, Instituto de Telecomunicações, University of Aveiro, Aveiro 3810-193, Portugal

DOI:10.1109/JPHOT.2017.2695522

Manuscript received March 29, 2017; revised April 12, 2017; accepted April 14, 2017. Date of publication April 19, 2017; date of current version May 19, 2017. This work was supported in part by the European Structural Investment Funds, through the Operational Competitiveness and Internationalization Programme (COMPETE 2020) under FutPON project [Nr. 003145 (POCI-01-0247-FEDER-003145)] and in part by the Fundação para a Ciência e a Tecnologia through the project COMPRESS, under Grant FRH/BPD/110889/2015. Correspondence author: Yahya Sheikhnejad (e-mail: yahya@ua.pt).

Abstract: In any wavelength sensitive application, extensive care should be taken in addressing the wavelength drift issues. In the case in which laser tuning is conducted by using thermoelectric cooler, an accurate expression is needed to describe transient characteristics of the Peltier device to achieve maximum controllability. In addition, thermal tuning issues are of particular relevance to the field of photonic integration. In this paper, the exact solution of the governing equation is presented, considering Joule heating, heat conduction, heat flux of the laser diode, and the thermoelectric effect in one dimension. In addition, the variable separation method and the Sturm–Liouville theorem, along with the completeness features of eigenfunctions, are used to obtain time-dependent electrical potential and temperature distribution of the Peltier device. Additionally, steady-state sensitivity analysis is performed in order to demonstrate the impacts of physical parameters on its thermoelectric characteristics. Transient temperature is also considered that, for a specific case, revealed fast transition to steady-state condition with time constant lower than 400 ms. Lower heat capacity, as well as laser diode heat flux, might lead to faster Peltier response times, such that the effect of heat flux on response time becomes negligible in low heat capacity Peltier.

Index Terms: Analytical solution, Peltier device, thermal management, transient analysis, laser thermal tuning.

1. Introduction

Current industrial tendencies strongly favor the concepts of low power consumption, high density, and low cost applications of Datacom and Telecom pluggable transceiver modules. Due to this point, thermal management, especially in the design of high-performance compact optical transceivers, plays an important role. Time-dependent wavelength drift derived from thermal agitation of direct modulated laser applies restriction on residency time for optical burst signals and hence has considerable influence on its application in dynamic optical networks [1]–[4]. Therefore, for the cost-sensitive thermally tuned laser diode (LD) in optical network units, the transient characteristics of the device need to be known.

Numerous efforts on numerical modeling of the transient and steady state thermal behavior of LDs have been reported [5]–[8], towards addressing their thermal tuning properties. By using COMSOL software and ignoring thermoelectric effect (Seebeck coefficient), Wang and Yu obtained distribution

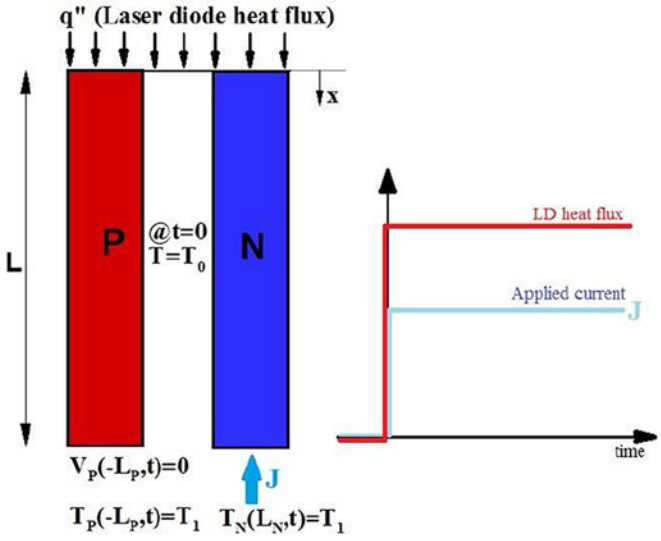

Fig. 1. (Left) Geometry and boundary condition of P-N junction and (right) LD heat flux and applied current during the time.

of temperature of sampled-grating distributed Bragg reflector (SG-DBR) over time [5]. Jaegle also used COMSOL software in his numerical work to simulate 3-D thermocouple by considering Peltier effect, whereby transient temperature is obtained from transient rectangular pulse of electrical current [6]. Mulvihill and O'Dowd proposed a transient model for tunable laser by ignoring Peltier effect and temperature distribution [7]. The latter considered a three-layer waveguide, laser chip and submount for their transient model, and used compensation technique to minimize the transition. Moreover, Meng *et al.* presented numerical transient simulation of 3-D thermoelectric cooler (TEC) [8]. The authors concluded that when current exceeds a specific value, the heat transferred from hot to the cold end by means of conduction will exceed the heat absorbed at the cold end via Peltier effect, thus the temperature at cold and hot ends increases continuously and the TEC is unable to reach the steady state. In addition, a number of investigations dedicated to the modeling of Peltier effect have been reported [9]–[19]. However, it is of note that in effort to add more detail to their approach, these works resort to iterative numerical methods, whereas their analytical solutions rely on a large number of limiting approximations. Additionally, numerical solutions have been studied for heat transfer in complex geometries containing heat conduction and forced convection as well [20], [21]. However, due to the benefits of closed-form exact solution, analytical approach would lead to a better understanding of thermal transient concept and potentially benefit the industry with higher controllability.

To achieve the goal of predicting the thermoelectric characteristics of Peltier device and obtain precise control over its behavior, an accurate closed-form expression is required. The most accurate description is the one obtained by exact solution of governing equation. Also, it is known that in order to analyze a system, one only needs to consider those directions with significant variation of dependent variable. In other words, considering extra dimensions at which there is negligible variation, may only result in complicated model with little additional gain. At the same time, it is essential to consider all effective parameters in the modeling. It can be concluded that as long as there is a negligible variation in one direction, simplified solution of 1-D analysis still provides a realistic approximation. Considering this point is crucial especially for the complicated systems such as complex configuration of thermoelectric cooler. In this study complete characteristics of Peltier device as an exact closed-form expression comprised of one dimensional transient Peltier considering Joule heating, heat conduction, heat flux of laser diode and thermoelectric effect is presented. Considered dimension in this study would be along the Peltier leg from top to bottom (see Fig. 1).

TABLE 1
Adopted Nomenclature and Definition of Variables. Var.: Variable, Sub.: Subscription

Var.	Unit	Description	Var.	Unit	Description
C_p	$(J/Kg.K)$	Specific heat capacity	T	(K)	Temperature
J	(A/m^2)	current flux	V	(V)	Voltage
k_{th}	$(W/m.K)$	Thermal cond	α	(V/K)	Seebeck coefficient
L	(m)	Length	α_t	(m^2/s)	Thermal diffusivity
q_e	(C/m^3)	Charge density	ρ	(Kg/m^3)	Density
q''	(W/m^2)	Heat flux	ρ_e	$(\Omega.m)$	Electrical resistivity
t	(s)	Time	σ	(S/m)	Electrical cond.
P, N	Sub.	P-type N-type	h	Sub.	homogeneous part
re, im	Sub.	real imaginary	ss	Sub.	steady state part

2. Governing Equation

Governing equations for the Peltier device are subjected to conservation of energy and electrical charge laws which in the general invariant form can be written as follows:

$$\nabla.(k_i \nabla T_i - \alpha_i T_i J) + \rho_{e,i} J^2 = \left(\rho C_p\right)_i \frac{\partial T_i}{\partial t} \quad i = P,\ N \tag{1}$$

$$T_P(x,t) \quad \& V_P(x,t) \quad -L_P \le x \le 0, \qquad t \ge 0$$

$$T_N(x,t) \quad \& V_N(x,t) \quad 0 \le x \le L_N, \qquad t \ge 0$$

$$\nabla.J = \frac{\partial q_e}{\partial t} \tag{2}$$

where electrical current density is given by

$$J = -\left(\sigma_i \vec{\nabla} V_i + \sigma_i \alpha_i \vec{\nabla} T_i\right) \quad i = P,\ N. \tag{3}$$

A set of non-linear Partial Differential Equations (PDEs) of (1)–(3) variables are defined in Table 1, together form the governing equations for two unknown variables of temperature and voltage, to describe the thermoelectric characteristics of Peltier device. This boundary value problem can be solved by Sturm-Liouville theorem and using new natural orthogonality relation and completeness features of eigenfunctions.

Here, we assume that there is negligible charge density accumulation [7]–[11], one-dimensional configuration and constant current and property. The logic behind this assumption is that charged density accumulation is matter only in an ultra-fast phenomenon. For the common application of Peltier device it can simply be ignored without deviation from reality.

We first consider the law of conservation of electrical charge, that under mentioned assumptions, is reduced to $\frac{\partial J}{\partial x} = 0$ which implies constant flux of electrical current along the given direction. Governing equation comprised of second order non-homogeneous PDE is subjected to non-homogeneous boundary conditions. It is assumed that the whole body is initially in the state of uniform temperature in (5), shown below, with new conditions instantaneously imposed on

boundaries

$$@t>0\begin{cases}T_P(-L_P,t)=T_1, & V_P(-L_P,t)=0\\ T_N(L_N,t)=T_2\\ T_P(0,t)=T_N(0,t), & V_P(0,t)=V_N(0,t)\\ k_P\frac{\partial T_P}{\partial x}\big|_{x=0}-k_N\frac{\partial T_N}{\partial x}\big|_{x=0}=q''_{LD}\end{cases} \tag{4}$$

$$@t=0,\qquad T_P(x,0)=T_N(x,0)=T_0,\qquad V_P(x,0)=V_N(x,0)=0. \tag{5}$$

At the one end (bottom), Peltier is adjacent to heat sink with infinite heat capacity which results in constant temperature and the other end (up) is subjected to heat flux of laser diode; see Fig. 1.

3. Solution Procedure

Due to the non-homogenous nature of PDE and its boundary conditions, we break down the variable into steady state and homogenous transient part such that

$$\begin{aligned}T_i(x,t) &= T_{i,ss}(x)+T_{i,h}(x,t), \qquad i=P,\ N.\\ V_i(x,t) &= V_{i,ss}(x)+V_{i,h}(x,t)\end{aligned} \tag{6}$$

The second term decays with time gradually toward zero, until it reaches the steady state. Details of derivation are given in the Appendix.

Therefore, the homogeneous part of temperature can be expressed as follows:

$$T_{p,h}(x,t)=\sum_{n=1}^{\infty}C_n e^{-a_t\lambda_n^2 t}e^{\frac{x}{2A_1}}\left(\tan(\beta_n L_P)\cos(\beta_n x)+\sin(\beta_n x)\right)$$

$$T_{N,h}(x,t)=\sum_{n=1}^{\infty}C_n f(\beta_n).e^{-a_t\lambda_n^2 t}e^{\frac{x}{2A_{1N}}}\times\left(-\tan\left(\sqrt{v_1\beta_n^2+v_2}.L_N\right)\cos\left(\sqrt{v_1\beta_n^2+v_2}x\right)+\sin\left(\sqrt{v_1\beta_n^2+v_2}x\right)\right)$$

$$f(\beta_n)=\frac{\tan(\beta L_P)\left(k_P\beta_{re,P}-k_N\beta_{re,N}\right)+k_P\beta}{k_N\sqrt{v_1.\beta^2+v_2}}. \tag{7}$$

Now, in order to apply the initial condition, steady state distribution of temperature for P- and N-type pillar is required. Non-homogeneous differential equations are given as

$$\frac{\partial}{\partial x}\left(\frac{\partial T_{i,ss}}{\partial x}-\frac{1}{A_{1,i}}T_{i,ss}\right)+\frac{\rho_e J^2}{k_i}=0 \tag{8}$$

$$\frac{\partial V}{\partial x}=-\left(\rho_e J+\alpha\frac{\partial T}{\partial x}\right). \tag{9}$$

Steady-state temperature and voltage are obtained by straight forward integration and application of non-homogeneous part of boundary conditions; see (4):

$$\begin{aligned}T_{i,ss}(x)&=\frac{x}{A_{2,i}}+K_{1,i}+K_{2,i}e^{\frac{x}{A_{1,i}}}\\ V_{i,ss}(x)&=-\frac{J}{\sigma_i}x-\alpha_i T_{i,ss}(x)+K_{3,i}\\ A_{1,i}&=\frac{k_i}{\alpha_i J},\ A_{2,i}=\frac{\alpha_i}{\rho_e J}.\end{aligned} \tag{10}$$

Furthermore, the coefficients $K_{1,i}$, $K_{2,i}$ and $K_{3,i}$ depend on boundary conditions which are given as

$$
\begin{aligned}
K_{1,P} &= T_1 + \frac{L_P}{A_{2,P}} - K_{2,P}.\, e^{\frac{-L_P}{A_{1,P}}} \\
K_{2,P} &= \frac{(T_2 - T_1) - \left(\frac{L_P}{A_{2,P}} + \frac{L_N}{A_{2,N}}\right) + \left(1 - e^{\frac{L_N}{A_{1,N}}}\right)\left(\frac{k_P}{k_N}\frac{A_{1,N}}{A_{2,P}} - \frac{A_{1,N}}{A_{2,N}} - \frac{A_{1,N}}{k_N} q''_{LD}\right)}{\left(1 - e^{\frac{-L_P}{A_{1,P}}}\right) - \left(1 - e^{\frac{L_N}{A_{1,N}}}\right)\frac{k_P}{k_N}\frac{A_{1,N}}{A_{1,P}}} \\
K_{1,N} &= T_2 - \frac{L_N}{A_{2,N}} - K_{2,N}.\, e^{\frac{L_N}{A_{1,N}}} \\
K_{2,N} &= \left[\frac{k_P}{k_N}\left(\frac{1}{A_{2,P}} + \frac{K_{2,P}}{A_{1,P}} e^{\frac{-L_P}{A_{1,P}}}\right) - \frac{q''_{LD}}{k_N} - \frac{1}{A_{2,N}}\right] A_{1,N} \\
K_{3.P} &= -\frac{J}{\sigma_P} L_P + \alpha_P.\, T_1 \\
K_{3,N} &= K_{3.P} + \left[\alpha_N\left(K_{1,N} + K_{2,N}\right) - \alpha_P\left(K_{1,P} + K_{2,P}\right)\right].
\end{aligned} \tag{11}
$$

Now, the application of initial condition for the homogeneous part of temperature results in

$$
\left[T_0 - T_{P,ss}(x)\right] = \sum_{n=1}^{\infty} C_n\, e^{\frac{x}{2A_1}} \left(\tan\left(\beta_n L_P\right)\cos\left(\beta_n x\right) + \sin\left(\beta_n x\right)\right) \tag{12}
$$

$$
\begin{aligned}
\left[T_0 - T_{N,ss}(x)\right] &= \sum_{n=1}^{\infty} C_n\, f\left(\beta_n\right).\, e^{\frac{x}{2A_{1N}}} \\
&\quad \times \left(-\tan\left(\sqrt{v_1\beta_n^2 + v_2}.\, L_N\right)\cos\left(\sqrt{v_1\beta_n^2 + v_2}\, x\right) + \sin\left(\sqrt{v_1\beta_n^2 + v_2}\, x\right)\right).
\end{aligned} \tag{13}
$$

Equations (12) and (13) show that an arbitrary function is described by summation of infinite eigenfunctions. This is commonly referred to as the "completeness" feature of a set of eigenfunctions which is the most important property of Sturm-Liouville solution. By using quasi-orthogonality [22] described by (14), unknown coefficient C_n can be obtained:

$$
k_N \int_{x=-L_P}^{0} \left[X_n X_m w(x)\right]_P dx + k_P \int_{x=0}^{L_N} \left[X_n X_m w(x)\right]_N dx = \delta_{nm}.\, N_n \tag{14}
$$

where N_n is referred to as the normalization integral or "Norm," which is given in (15), while δ_{nm} is the Kronecker delta function

$$
N_n = k_N \int_{x=-L_P}^{0} \left[X_n^2 w(x)\right]_P dx + k_P \int_{x=0}^{L_N} \left[X_n^2 w(x)\right]_N dx. \tag{15}
$$

We next multiply both side of (12) by k_N and integrate from $-L_P$ to 0, whereas (13) is multiplied by k_P and integrated from 0 to L_N. Thereafter, the homogeneous part of voltage can be obtained

TABLE 2
Material Properties Used in the Analysis

P-type	$C_p = 100$	$\sigma = 1.0e5$	$k_{th} = 1.0$
	$\rho = 7700$	$L = 0.6e-3$	$\alpha = 200e-6$
N-type	$C_p = 100$	$\sigma = 1.0e5$	$k_{th} = 1.0$
	$\rho = 7700$	$L = 0.6e-3$	$\alpha = -200e-6$

by direct integration, as follows:

$$V_{p,h}(x,t) = -\alpha_P . \sum_{n=1}^{\infty} C_n\, e^{-a_t \lambda_n^2 t}\, e^{\frac{x}{2A_1}} \left(\tan(\beta_n L_P)\cos(\beta_n x) + \sin(\beta_n x)\right) + K_{4,P}$$

$$V_{N,h}(x,t) = -\alpha_N \sum_{n=1}^{\infty} C_n\, f(\beta_n) . e^{-a_t \lambda_n^2 t}\, e^{\frac{x}{2A_{1N}}} \times \left(-\tan\left(\sqrt{v_1\beta_n^2 + v_2}.L_N\right)\cos\left(\sqrt{v_1\beta_n^2 + v_2}x\right) + \sin\left(\sqrt{v_1\beta_n^2 + v_2}x\right)\right) + K_{4,N}$$

$$K_{4,P} = 0, \qquad K_{4,N} = (\alpha_N - \alpha_P) . T_{h,P}(0,t) . \tag{16}$$

Finally, the set formed by (16), (10), (7), and (6) describes complete transient behavior of Peltier.

4. Result and Discussion

This section presents the results of our analytical approach. Sensitivity analysis in the steady-state condition are discussed first, followed by the results of transient condition.

4.1 Sensitivity Analysis

In order to assess the effect of each variable on the performance of P-N junction and its thermoelectric characteristics, steady-state sensitivity analysis is performed. Base values used are summarized inTable 2.

It should be noted that in the figures presented hereafter, the relation between x and X is $X = x + L_P\,[0 \le X \le (L_P + L_N)]$ where the interval $0 < X < 0.6$ mm refers to the distribution of dependent variable in the P-type pillar, and $0.6 < X < 1.2$ mm to that of N-type pillar. Additionally, both x and X axis are considered in the same direction. Moreover, we hereby consider $T_1 = T_2 = 300\,K$ and $L_P = L_N = L = 0.6\,\text{mm}$. In addition, it is good to mention that heating and cooling in the P-N junction occur when the junction (common point of P- and N- pillar in the upper part) obtains temperature higher and lower than that of the base pillar (lower part), respectively.

We first consider thermal and electrical conductivity, which are presented in Figs. 2 and 3, respectively. As can be noted, thermal conductivity has a negligible effect on voltage but highly affects the temperature distribution. It has the effect of reducing the temperature difference towards uniform distribution. Moreover, as shown in Fig. 2, when the direction of electrical current is the same as that of x (or X) axis (i.e. positive current) the P-N junction will be in the heating mode, whereas when current is negative, it will enter the cooling mode. Positive and negative current will further result in negative and positive gradient in voltage distribution, respectively. Fig. 3 shows the sensitivity of voltage and temperature to an electrical conductivity. In contrast to thermal conductivity, voltage is highly sensitive to variation of electrical conductivity, such that for a same level of current, higher conductivity leads to a lower differential potential.

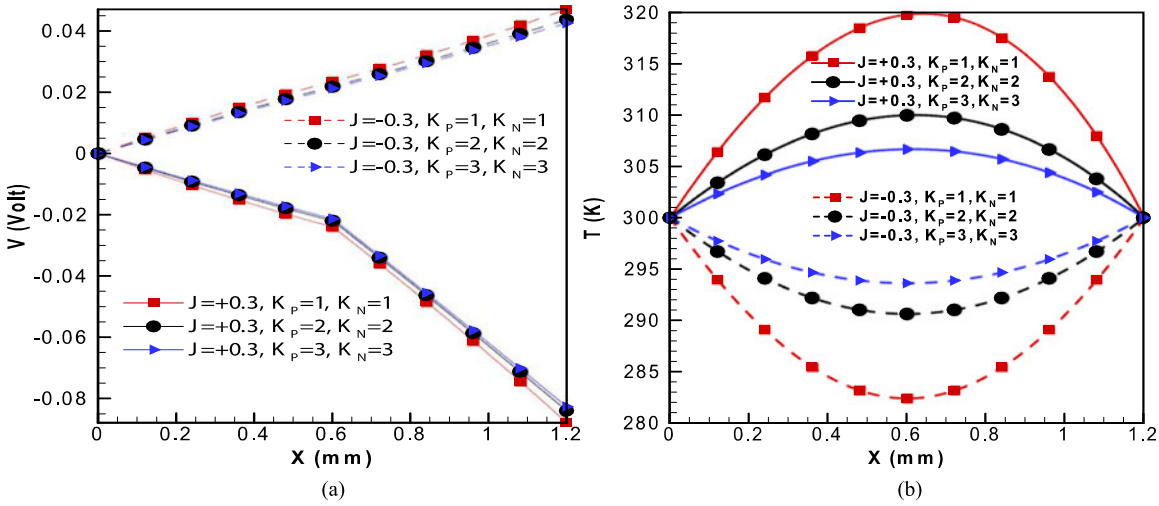

Fig. 2. Effect of thermal conductivity on the distribution of (a) voltage and (b) temperature without heat load.

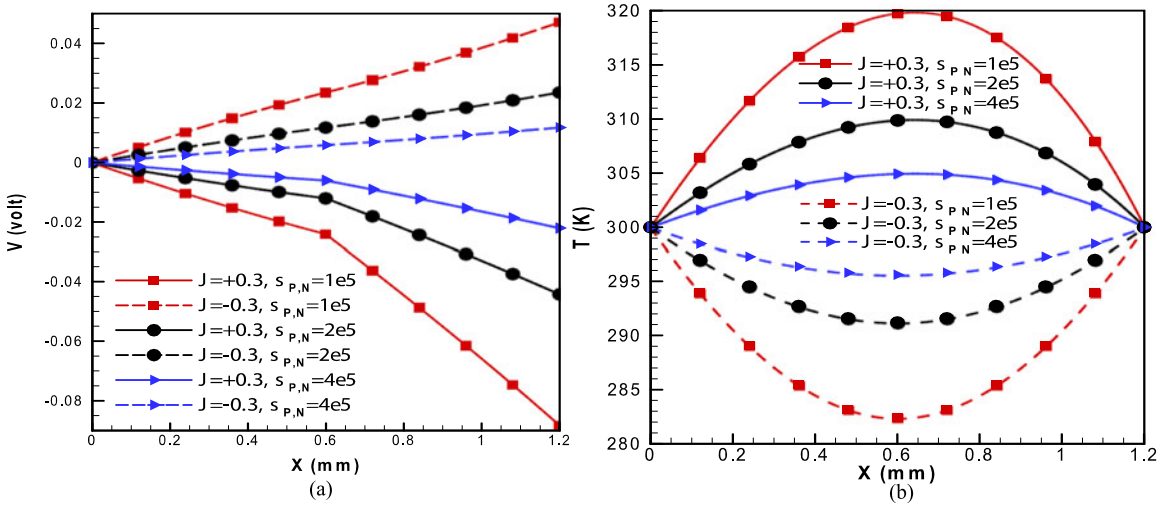

Fig. 3. Effect of electrical conductivity on the distribution of (a) voltage and (b) temperature without heat load.

Also, by increasing electrical conductivity, resistivity of material and joule heating decreased, and hence temperature difference decreases as well. When Peltier is used for the purpose of cooling down the LD, especially at a high bit rate producing high heat flux, P-N junction will be in the cooling mode, and it is required to consume much more electrical power to reduce the temperature of LD. The latter is supported by the result presented in Fig. 4. Evidently, with growing current the differential voltage is also increased, following a quasi-linear dependency.

In Fig. 5, effect of imbalance property on P- and N- type pillar is shown and proven to have disruptive effect on the symmetric distribution of temperature. Due to the fact that heat flux is conserved at the common junction point, the difference in conductivity will lead to a difference in temperature gradient, meaning that temperature curve will be discontinued at the junction. Moreover, by changing imbalance of properties, the temperature curves are mirrored with respect to the junction plane, whereas temperature and potential difference are not affected at all.

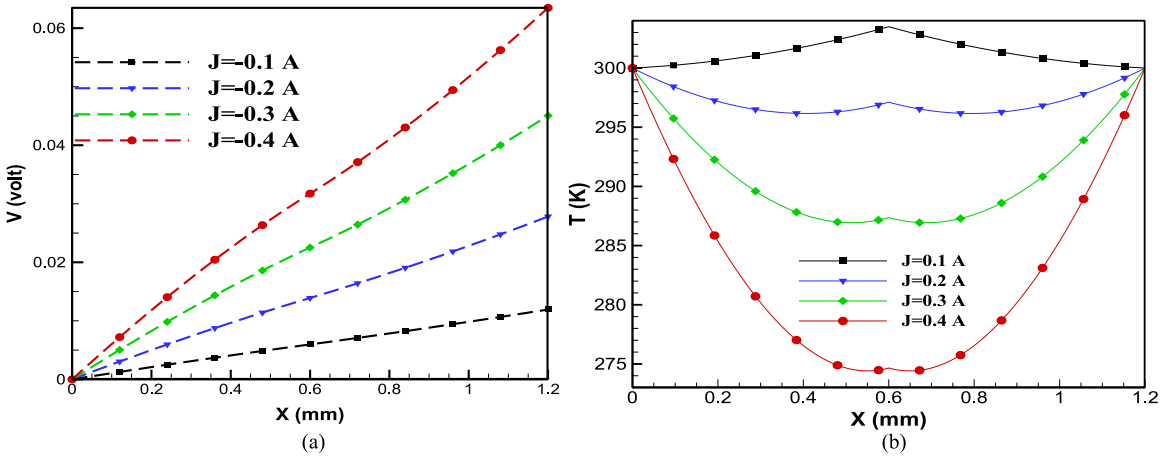

Fig. 4. Effect of current on the distribution of (a) voltage and (b) temperature with heat load.

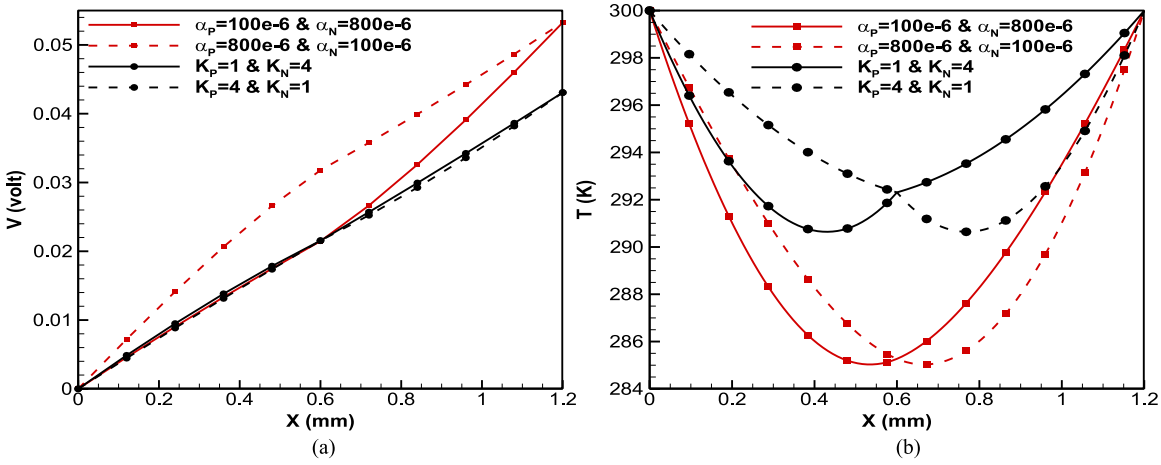

Fig. 5. Effect of property imbalance on the distribution of (a) voltage and (b) temperature without heat load.

4.2. Transient Results

The transient analysis of 1D Peltier device and effect of LD heat load is presented in Fig. 6. Due to the importance of management of high heat flux, transient behavior of Peltier device is compared in presence and in absence of LD heat load. Also, here, 2 mW LD is considered as a source of heat flux and a Peltier of 1 mm^2 cross section area which together lead to the high heat flux of 20 mW/mm^2 or in SI unit: 20 KW/m^2. Obviously, this heat flux value could be true for the Peltier size of 0.1 mm^2 and LD power of 2 W. In order to provide sufficient level of accuracy, resolution of time steps was set to 1 ms. First of all, temporal evolution of whole the Peltier device in a several time sections shows its fast response. It is of note that considering junction point temperature, the time constant of the Peltier considered here is approximately 80 ms. Moreover, in Fig. 6(a), the temperature curve and its gradient are continuous at each time level, meaning that boundary conditions are completely satisfied.

In addition, LD heat flux has no effect on the rate of Peltier response, however it will decrease the temperature difference and increase cooling temperature in cooling mode. In other words cooling mode will occur at higher temperature and at the location other than the junction point. Moreover, due to the fact that extra heat flux from outsource is added to the junction point, although thermal conductivities are equal, the curve exhibits broken point at the added (junction) point.

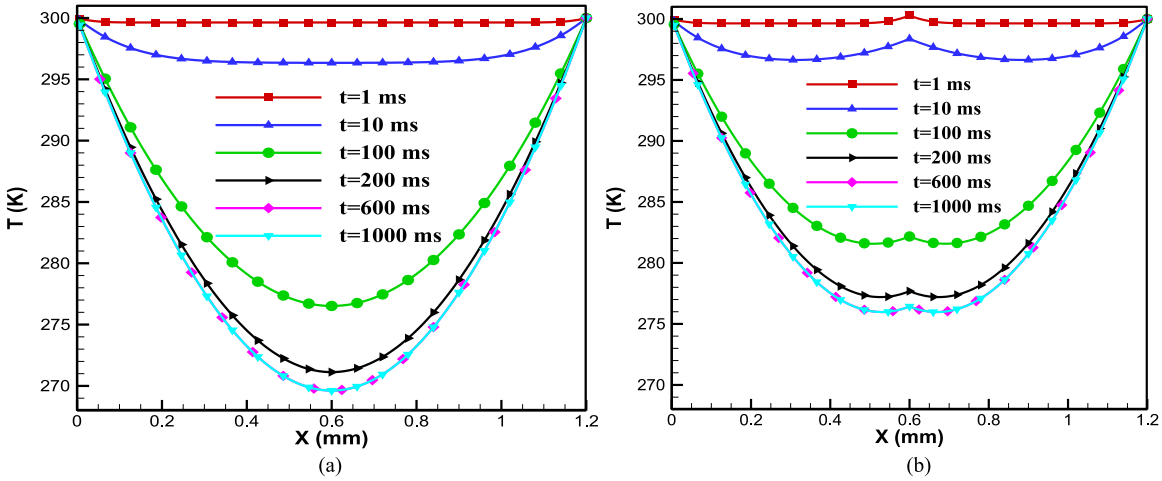

Fig. 6. Transient temperature behavior for several time sections. (a) Without heat LD heat flux. (b) With LD heat flux ($J = -0.37\,A$, $\sigma = 0.6 \times 10^5$, $k_{th} = 1.5$).

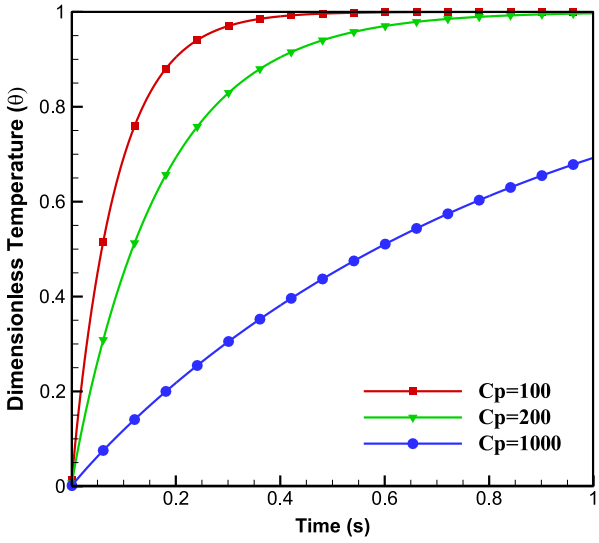

Fig. 7. Dimensionless mean temperature of Peltier during the time for three different heat capacities. ($J = -0.37\,A$, $\sigma = 0.6 \times 10^5$, $k_{th} = 1.5$)

In order to have a better understanding of Peltier transient behavior, averaged temperature and dimensionless averaged temperature θ, defined in (17), is depicted in Figs. 7 and 8. In fact, Fig. 7 presents the averaged response of Peltier device to its external excitation, Fig. 1 (right). As it can be seen, higher heat capacity results in slower response so that for the applications that rely on faster response, materials with lower heat capacity have to be used. The curve for Cp $=$ 100 respect to the curve for Cp $=$ 1000 can reaches to the steady state faster. Also increasing heat capacity two times from 100 to 200 will result in two times slower response to the external excitation. For the material with high heat capacity, such as $C_p = 1000$, the steady state will not be reached in 1 second interval time. Fig. 7 also shows that fast response of considered Peltier results in steady state condition within less than 400 ms and that most of the temperature change occurred within only 150 ms interval. In Fig. 8, averaged temperature under four different conditions were compared which approved Fig. 7 as well. Again, faster response of lower heat capacity Peltier to reach steady state is evident. In addition, LD heat load of 2 mW increases temperature by 10 degrees. However,

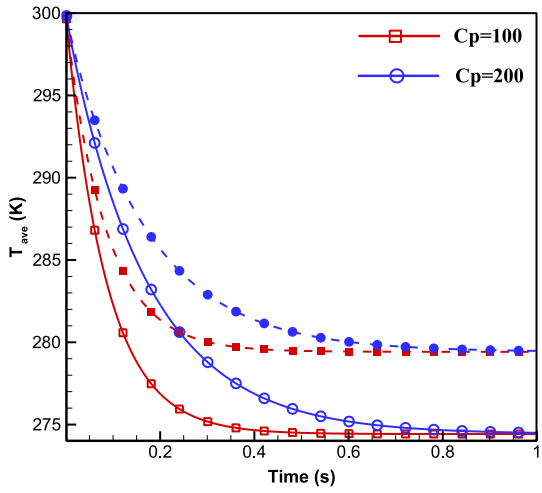

Fig. 8. Averaged temperature of Peltier during the time for three different heat capacities. Solid lines + open markers: without heat load. Dashed lines + filled markers: with heat load ($J = -0.37\,A$, $\sigma = 0.6 \times 10^5$, $k_{th} = 1.5$).

heat load effect on transient response, although negligible, but somehow in the way to make it faster

$$\theta = \frac{\bar{T}(t) - T_0}{\bar{T}_{ss} - T_0}$$

$$\bar{T}(t) = \frac{1}{L_P}\int_{-L_P}^{0} T_P(x,t)\,dx + \frac{1}{L_N}\int_{0}^{L_N} T_N(x,t)\,dx. \tag{17}$$

5. Conclusion

In this work, transient analytical closed-form expression as an exact solution of governing equation presented with the aim of describing thermoelectric characteristics of Peltier device using separation of variables and Sturm-Liouville theorem. Negligible charge density accumulation, one-dimensional configuration and constant current and property were assumed. Steady state sensitivity analysis reveals that heat flux from LD and thermal conductivity have a negligible effect on voltage distribution but highly affect the thermal behavior of Peltier. On the other hand, electrical current and conductivity have a significant effect on variation of voltage as well as temperature distribution. Moreover, studied Peltier device has a fast response such that the steady state condition is achieved in less than 400 ms. Also, LD heat flux up to 20 mW/mm^2 increases cooling temperature up to 7 °C. Finally, it is important to note that in this scientific area, analytic approach will be too sophisticated to solve if one wants to add fine details to the configuration. However, benefits of closed form analytical solution for programming actuators in photonic integrated circuit are worthwhile enough to take into consideration. Future work will be dedicated to adding further detail to this model and generalizing it in terms of the assumptions adopted in this particular work.

Appendix

All non-homogeneities are assigned to the steady-state part, and thus, the homogeneous part will entail only homogeneous boundary conditions:

$$\begin{cases} \frac{\partial}{\partial x}\left(\frac{\partial T_{i,h}}{\partial x} + \frac{1}{A_{1,i}}T_{i,h}\right) = \frac{1}{\alpha_{t,i}}\frac{\partial T_{i,h}}{\partial t} \quad i = P, N \\ A_{1,i} = \frac{k}{\alpha J}, \qquad \alpha_{t,i} = \left(\frac{k}{\rho C}\right)_i. \end{cases} \tag{A1}$$

Toward obtaining the solution, we first separate the variables

$$\begin{cases} T_{i,h}(x,t) = X_i(x).\,\Gamma_i(t), & i = P,\ N \\ T_{i,h}(x,0) = T_0 - T_{i,ss}(x) \end{cases} \tag{A2}$$

which, by substituting into (7), gives

$$\dot{\Gamma}_i + \alpha_{t,i}\lambda^2\Gamma_i = 0 \tag{A3}$$

$$X_i'' - \frac{1}{A_{1,i}}X_i' + \lambda^2 X_i = 0 \tag{A4}$$

where coefficient λ is the separation constant for the boundary value problem, described by (A1). Characteristic equation for (A4) is solved for two distinct values:

$$D_{1,2} = \frac{1 \pm \sqrt{\Delta}}{2A_{1,i}}, \qquad \Delta = 1 - 4A_{1,i}^2\lambda^2. \tag{A5}$$

Considering boundary conditions, (4), only trivial solution will be obtained when $\Delta > 0$ or $\Delta = 0$. Moreover, (A4) can be written in the form of self-adjoint (Sturm-Liouville) as follows:

$$\frac{d}{dx}\left(e^{\frac{-x}{A_{1,i}}}X'_i\right) + \lambda^2 e^{\frac{-x}{A_{1,i}}}X_i = 0 \tag{A6}$$

where weight function is given as $w(x) = \exp(\frac{-x}{A_{1,i}})$. The aforementioned weight function is addressed as a part of discussion on the orthogonality feature of eigenfunctions.

For $\Delta < 0$ solution of (A3) and (A4) can be given as

$$\Gamma_i(t) = e^{-\alpha_{t,i}\lambda_i^2 t} \tag{A7}$$

$$\begin{cases} X_i(x) = a_i e^{(\beta_{re}+j\beta_{im})x} + b_i e^{(\beta_{re}+j\beta_{im})x} = e^{\beta_{re}}\left(a_i\cos(\beta_{im}x) + a_i\sin(\beta_{im}x)\right) \\ j = \sqrt{-1}, \quad \beta_{re} = \frac{1}{2A_{1,i}},\ \beta_{im} = \frac{\sqrt{4A_{1,i}^2\lambda_i^2 - 1}}{2A_{1,i}}, \qquad i = P, N. \end{cases} \tag{A8}$$

Upon the application of boundary conditions, (4), we further obtain

$$\begin{cases} a_P = \tan(\beta_{im,P}L_P)\,b_P \\ a_N = -\tan(\beta_{im,N}L_N)\,b_N \\ a_P e^{-\alpha_{t,P}\lambda_P^2 t} = a_N e^{-\alpha_{t,N}\lambda_N^2 t} \\ k_P(a_P\beta_{re,P} + b_P\beta_{im,P}) = k_N(a_N\beta_{re,N} + b_N\beta_{im,N}) \end{cases} \tag{A9}$$

which further implies that

$$\begin{cases} a_P = a_N \\ \frac{\lambda_P^2}{\lambda_N^2} = \frac{\alpha_{t,N}}{\alpha_{t,P}} = \frac{A_{1,N}^2}{A_{1,P}^2}\frac{\sqrt{4A_{1,P}^2\beta_{im,P}^2+1}}{\sqrt{4A_{1,N}^2\beta_{im,N}^2+1}}. \end{cases} \tag{A10}$$

From (A9) and (A10), the relation between eigenvalue of two parts of Peltier device (P- and N-pillars) is obtained as follows:

$$\begin{cases} \beta_{im,N}^2 = v_1\beta_{im,P}^2 + v_2 \\ v_1 = \frac{4A_{1,P}^2}{4A_{1,P}^2 u}, \qquad v_2 = \frac{1-u}{4A_{1,P}^2 u}, \quad u = \frac{\alpha_{t,N}}{\alpha_{t,P}}.\frac{A_{1,P}^2}{A_{1,N}^2}. \end{cases} \tag{A11}$$

Next, by combining (A9) and (A10), the following relation between the unknown coefficients can be obtained:

$$b_N = b_P \frac{\tan\left(\beta_{im,P} L_P\right)\left(k_P \beta_{re,P} - k_N \beta_{re,N}\right) + k_P \beta_{im,P}}{k_N \sqrt{v_1 . \beta_{im,P}^2 + v_2}} \tag{A12}$$

$$b_N = b_P \frac{k_P\left(\beta_{im,P} + \beta_{re,P} . \tan\left(\beta_{im,P} L_P\right)\right)}{k_N\left(\beta_{im,N} + \beta_{re,N} . \tan\left(\beta_{im,N} L_N\right)\right)}. \tag{A13}$$

In fact, (A12) and (A13) would be equivalent to each other but in a different form and the eigenvalues are the roots of transcendental equation (20):

$$\beta_{im,P} = \beta = \frac{k_N . \sqrt{v_1 . \beta^2 + v_2} . \tan\left(\beta L_P\right)}{k_P . \tan\left(\sqrt{v_1 . \beta^2 + v_2} . L_N\right)} + \tan\left(\beta . L_P\right) . \left(\beta_{re,P} - \frac{k_N}{k_P} \beta_{re,N}\right). \tag{A14}$$

Additionally, only when the separation constant equals to eigenvalue, differential (A4) has a non-trivial solution and general solution can be the summation of all individual solutions corresponding to each eigenvalue.

References

[1] *40-Gigabit-Capable Passive Optical Networks 2 (NG-PON2): Physical Media Dependent (PMD) Layer Specification*, ITU-T G989.2, 2015.

[2] G. Y. Chu and J. Prat, "Ultrafast wavelength jumping and wavelength adjustment with low current using monolithic integrated FML for long-reach UDWDM-PON," *IEEE Photon. J.*, vol. 8, no. 6, pp. 1–9, 2016.

[3] G. Simon *et al.*, "Focus on time-dependent wavelength drift of DMLs under burst-mode operation for NG-PON2," *J. Lightw. Technol.*, vol. 34, no. 13, pp. 3148–3154, Jul. 2016.

[4] Y. Su, J. E. Simsarian, and L. Zhang, "Improving the switching performance of a wavelength-tunable laser transmitter using a simple and effective driver circuit," *Photon. Technol. Lett.*, vol. 16, no. 9, pp. 3132–3134, 2004.

[5] H. Wang and Y. Yu, "New theoretical model to analyze temperature distribution and influence of thermal transients of an SG-DBR laser," *J. Quantum Electron.*, vol. 48, no. 2, pp. 107–113, 2012.

[6] M. Jaegle, "Multiphysics simulation of thermoelectric system—Modeling of Peltier cooling and thermoelectric generator," in *Proc. COMSOL Conf.*, 2008, pp. 4–6.

[7] G. Mulvihill and R. O'Dowd, "Thermal transient measurement, modeling, and compensation of a widely tunable laser for an optical switched network," *J. Lightw. Technol.*, vol. 23, no. 12, pp. 4101–4109, Dec. 2005.

[8] J. Meng, X. Wang, and X. Zhang, "Transient modeling and dynamic characteristics of thermoelectric cooler," *J. Appl. Energy*, vol. 108, pp. 340–348, 2013.

[9] B. V. K. Reddy, M. Barry, J. Ki, and M. K. Chyu, "Three dimensional multiphysics coupled field analysis of an integrated thermoelectric device," *J. Numer. Heat Transfer, Part A*, vol. 62, pp. 933–947, 2012.

[10] B. V. K. Reddy, M. Barry, J. Ki, and M. K. Chyu, "Mathematical modeling and numerical characterization of composite thermoelectric device," *Int. J. Therm. Sci.*, vol. 67, pp. 53–63, 2013.

[11] M. Chen, L. A. Rosendahl, and T. Condra, "A three dimensional numerical model of thermoelectric generators in fluid power system," *Int. J. Heat Mass Transfer*, vol. 54, pp. 345–355, 2011.

[12] T. Ming *et al.*, "The influence of non-uniform high heat flux on thermal stress of thermoelectric power generator," *J. Energies*, vol. 8, pp. 12584–12602, 2015.

[13] R. Bjork, D. V. Cheristensen, D. Eriksen, and N. Pryds, "Analysis of the internal heat losses in a thermoelectric generator," *Int. J. Therm. Sci.*, vol. 85, pp. 12–20, 2014.

[14] J. Garcia-Canadas and G. Min, "Thermal dynamics of thermoelectric phenomena from frequency resolved methods," *AIP Adv.*, vol. 6, 2016, Art. no. 035008.

[15] F. X. Villasevil, A. M. Lopez, and M. Fisac, "Modeling and simulation of a thermoelectric structure with pellets of non-standard geometry and materials," *Int. J. Refrigeration*, vol. 26, pp. 1570–1575, 2013.

[16] J.-Y. Li, Z.-H. Du, Y.-W. Ma, and K.-X. Xu, "Dynamic thermal modeling and parameter identification for a monolithic laser diode module," *J. Chin. Phys. B*, vol. 22, no. 3, 2013, Art. no. 034203.

[17] H. Tsai and J. Lin, "Model building and simulation of thermoelectric module using matlab/simulink," *J. Electron. Mater.*, vol. 39 no. 9, pp. 2105–2111, 2009.

[18] D. Yan, "Time dependent finite volume model of thermoelectric device," *IEEE Trans. Ind. Appl.*, vol. 50, no. 1, pp. 600–608, Jan./Feb. 2014.

[19] T. Ming, Y. Wu, C. Peng, and Y. Tao, "Thermal analysis on a segmented thermoelectric generator," *J. Energy*, vol. 80, pp. 388–399, 2015.

[20] Y. Sheikhnejad, R. Hosseini, and M. S. S. Avval, "Experimental study on heat transfer enhancement of laminar ferrofluid flow in horizontal tube partially filled porous media under fixed parallel magnet bars," *J. Magn. Magn. Mater.*, vol. 424, pp. 16–25, 2017.
[21] Y. Sheikhnejad, R. Hosseini, and M. Saffar-avval, "Laminar forced convection of ferrofluid in a horizontal tube partially field with porous media in the presence of magnetic field," *J. Porous Media*, vol. 18, no. 4, pp. 437–448, 2015.
[22] C. W. Tittle, "Boundary value problems in composite media: quasi-orthogonal functions," *J. Appl. Phys.*, vol. 36, no. 4, pp. 1486–1488, 1965.